Satellite Doppler Determination of Differential Sea Ice Motion in the Vicinity of the North Pole*

J. Popelar

J. Kouba

Department of Energy, Mines & Resources
Earth Physics Branch
Gravity, Geothermics & Geodynamics Division
1 Observatory Crescent
Ottawa, Canada K1A OY3

Abstract During April and May 1979 multidisciplinary observations were conducted in the central Arctic Ocean from three manned ice stations to explore the nature of the submarine Lomonosov Ridge (Weber, 1979). Positions of the LOREX (Lomonosov Ridge Experiment) ice camps were monitored continuously using geodetic satellite doppler receivers and the U.S. Navy Navigation Satellite System. Near real-time doppler data reduction on the ice using broadcast satellite ephemeris provided operational horizontal positions with accuracies of about ± 250 m. A precise geodetic satellite doppler reduction program has been adapted to accommodate linear station motion in a simul-

*Contribution of the Earth Physics Branch No. 1036; Lorex Contribution No. 14.

Marine Geodesy Vol. 7, Number 1-4
0149-0419/83/030171-00$02.00/0
Copyright © 1983 Crane, Russak & Company, Inc.

BOREAL INSTITUTE LIBRARY
54670

Pam:551.326.14:(*301) POP

POLAR PAM 2049

POLARPAM

taneous multistation, three-dimensional adjustment in phases using postfitted precise satellite ephemeris, if available. Complete reprocessing of the LOREX doppler data set has produced average errors of ± 48 m for single pass solution and ± 24 m for mean three-four horizontal station positions. The station ellipsoidal heights show strongly correlated variations in excess of 5 m, with the average error of ± 0.45 m. Station velocities are also strongly correlated, with the mean of about 225 m/h and the maximum of 1,240 m/h. Total strain and hourly strain rate components of sea ice have been evaluated for a homogeneous two-dimensional strain model. The configuration of the ice camps provides a unique solution for mesoscale strain, indicating a major change in the pattern of pack ice deformation over the Lomonosov Ridge. The total strain reflects plastic deformation, which takes place mainly in episodic events. The strain rate also indicates nearly diurnal oscillations, with amplitudes an order of magnitude smaller than those corresponding to the major deformation events.

Introduction

The Lomonosov Ridge Experiment code, named LOREX 79, was organized by the Earth Physics Branch in cooperation with the Polar Continental Shelf Project. This multidisciplinary expedition to explore the nature and origin of the major submarine mountain ridge bisecting the Arctic Ocean between the Canadian and Siberian continental shelves took place in the spring of 1979 when geophysicists, geologists, and oceanographers carried out measurements from the drifting sea ice, took samples, and studied the ocean floor in the vicinity of the geographical North Pole. Three permanent ice camps—the Base Camp, Snowsnake, and Iceman—forming approximately an isosceles triangle with sides of about 60-km long and a 100-km base served as operation bases during the experiment (Weber, 1979). The ice camps were established upstream of the narrowest portion of the Lomonosov Ridge, and it was expected that the Transpolar Current would carry them across the ridge with an average speed of about 5 km per day. With known irregularities of sea ice drift it was essential to the success of the expedition to provide reliable all-weather positioning of the ice camps with the highest achievable accuracy. The Navy Navi-

gation Satellite System, also known as Transit, was the only system capable of providing real-time navigation to support field operations at the ice camps with a potential for further substantial improvement of the positional accuracy using postfitted precise satellite ephemeris and highly refined doppler data reduction software.

Although the Transit system facilitates accurate navigation of vessels on high seas and precise geodetic positioning of points on the earth's surface at latitudes up to 70°, the polar orbits of the Transit satellites give rise to two undesirable effects in the vicinity of the geographic poles: (1) every orbit of every satellite of the system is visible, producing at times severe mutual interference degrading the data quality; and (2) all the satellites pass nearly overhead, resulting in poor fix geometry and, moreover, frequent loss of signal at closest approach due to the tracking antennae gain pattern. These effects are particularly severe during unattended operation of standard Transit satellite receivers.

Satellite positions of the LOREX Base Camp were evaluated in real time with the satellite receiver on line to a disc-based minicomputer system most of the time. Raw satellite data from Snowsnake and Iceman camps were recorded on magnetic cassettes, which were then processed on the main camp computer with a three- to seven-day delay. The two-dimensional satellite fix evaluation software developed for BIONAV has been used to process the data on the ice during the expedition (Wells, 1976; Wells and Grant, 1977). At the same time copies of the raw and majority voted data files have been preserved on seven-track magnetic tapes for further analysis and postprocessing (Popelar et al., 1981).

A precise geodetic satellite positioning software package GEODOP (Kouba and Boal, 1976) has been modified extensively to accommodate sequential simultaneous positioning of slowly moving stations. The program employs higher order modeling of environmenal and instrumental effects, reflects time and space correlation of model parameters during simultaneous tracking from several stations, and takes advantage of the availability of postfitted precise satellite orbits. Thus, much improved positions of the LOREX camps have been obtained in three dimensions to satisfy the precision requirements of the plumb-line deflection ex-

periment (Johnson, 1982). The improved positions have made it possible to evaluate differential motion of the three stations and provide a unique solution for two-dimensional strain of the sea ice during the LOREX expedition. The results are particularly valuable, since for the first time variations of ellipsoidal height for the ice stations can be correlated with horizontal sea ice strain components. Analysis of the vertical coordinate provides information on variations of sea surface topography in the central Arctic Ocean.

Satellite Dynamic Positioning

Although the real-time satellite navigation satisfied well the operational requirements on the ice and provided positions acceptable for most of the scientific projects carried out during the LOREX expedition, the plumb-line deflection experiment required satellite positions to about ± 30 m to match the expected accuracy of astro fixes. High-precision satellite doppler positions are routinely obtained by multipass multistation solutions, based on postfitted satellite ephemeris, at 1 to 2 m level for geodetic purposes. However, geodetic models assume earth-fixed stations, whereas motion of an ice station can be appreciable and has to be modeled accordingly.

The new dynamic doppler reduction program GERDOP uses comprehensive error modeling of instrumental, orbital, and environmental effects for simultaneous multistation three-dimensional adjustment in phases (Kouba, 1979, 1981). Several program modules have been modified or completely rewritten to accommodate station position and velocity variations under the assumption of linear station motion over specified equal-length time intervals. Selection of the time interval is crucial; it has to be short enough to permit a linear approximation of the true motion and provide for accumulation of sufficient number of satellite passes to determine mean station positions and linear velocities. The station motion is modeled by three independent linear fits to successive station latitude, longitude, and height coordinates weighted according to their formal errors. A new linear fit is initiated at the beginning of each interval, and departures from the least-

squares line are modeled as exponentially correlated time processes in both the station coordinates and velocities to reflect the strong positive correlation of station positions over short time intervals. The doppler data reduction model accepts only dual-frequency data, corrects for higher order ionospheric effects, and respects the time and space correlation of the tropospheric refraction scaling factors and correlation between doppler data and model parameters during simultaneous tracking from several stations. Reference orbit bias is obtained from the simultaneous solution for each satellite pass, with parameter weights providing desirable constraints. A sequential adjustment procedure is used to update station positions, velocities, model bias parameters, and corresponding variance–covariance matrices after each pass. In this way only new observations are processed to update results of previous solutions without the loss of continuity, thus greatly increasing the economy of computation. Linear extrapolation is used to initialize interval mean station positions and velocities, using time- and space-dependent exponential correlation functions.

Postprocessing of the LOREX satellite doppler data is based on majority-voted output obtained during the real-time navigation preprocessing. Table 1 gives statistics for the LOREX dynamic positioning. The total of 4,920 passes from the three stations that have passed the preprocessing data quality checks represents 2,700 passes of one of the five operational satellites. This means that each accepted satellite pass was tracked at an average by two of the three LOREX stations, thus effectively taking advantage of the simultaneous multistation solution. The very low pass rejection rate increases by 20% the overall data recovery in comparison with the real-time navigation. Orbital data for satellites 12 and 20 (1,064 passes) have been derived from the broadcast message in a similar way as for the navigation processing, whereas precise postfitted orbits provided by the U.S. Defense Mapping Agency have been used for satellites 13, 14, and 19 (1,636 passes). This has significant impact on the point-positioning accuracy: the predicted broadcast orbits provide satellite positions in ± 20–30 m range, whereas the accuracy of the precise ephemeris is ± 2 m. The sequential adjustment of consecutive passes for which ground tracks change direction rapidly in the vicinity of the geographic pole

Table 1
Summary of LOREX dynamic positioning.

	Main Camp	*Snowsnake*	*Iceman*	*Total*
Station ID	S0	S1	S2	
Passes tracked	3,352	2,153	1,940	7,445
computed	2,189	1,368	1,363	4,920
accepted	2,162	1,334	1,340	4,836
Accepted per day	37.2	29.9	30.5	97.6
Data recovery	64%	62%	69%	65%
Pass rejection rate	1.2%	2.5%	1.7%	1.7%

practically eliminates the effect of larger cross-track errors produced by the overhead geometry. Moreover, the simultaneous multistation solution increases the accuracy of relative station positions, which is significant for evaluation of the differential station motion and studies of pack ice dynamics.

Mean polar stereographic coordinates of the LOREX stations as obtained by the dynamic positioning software for three-hour intervals are shown in Figure 1. The overall average error of the mean positions is ± 24 m in latitude and longitude and ± 0.42 m in ellipsoidal height. These estimates are somewhat conservative, since the first ten days of doppler data (day 92 to day 102) show much higher noise due to an initial oscillator instability producing much greater formal errors; the height solution is most sensitive and had to be practically fixed for that period. It is correct to say that errors in mean positions vary from interval to interval depending on the amount of data, pass geometry, and character of ice motion; errors under ± 15 m are encountered about 40% of the time.

Figure 2 displays the station velocities and their directions rections with respect to the Greenwich meridian. It is apparent that motion of the three stations is strongly correlated, reflecting relative rigidity of the sea ice cover at scales of 100 km. The average station velocity during LOREX was about 225 m/h reaching a maximum of 1,240 m/h on day 124. The direction of motion changed rapidly at times showing rather large scatter for low velocities, but the prevailing direction was about 190° with respect to the Greenwich meridian. Accumulated track length for the Main

Camp was 304.6 km, whereas Snowsnake and Iceman track lengths were 241.4 km and 240.6 km, respectively. The direct separations between the starting and terminal points for the three stations are 149.8 km, 140.6 km, and 158.6 km. The LOREX pass summary file is available on magnetic tape and lists receiver frequency offset, cartesian and geodetic coordinates, velocity, and separation between stations from simultaneous tracking for the 4,836 individual pass station solutions.

The standard errors for latitude, longitude, height, and station separation are derived directly from the solution variance–covariance matrix, which also reflects in addition to data quality and pass geometry the constraints imposed by the time- and space-dependent exponential correlation functions used for modeling physically realistic conditions from pass to pass. The mean errors for the pass solutions are about ± 48 m for latitude and longitude, ± 0.45 m for height, and ± 43 m for station sep-

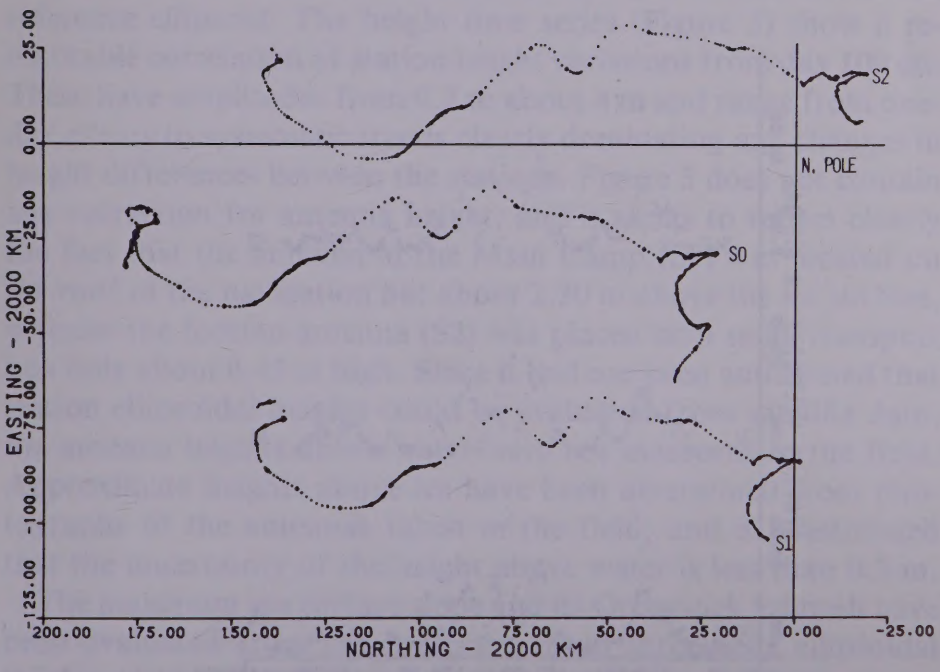

Figure 1. Mean three-hour LOREX ice camp positions. S0 = Main Camp, S1 = Snowsnake, S2 = Iceman.

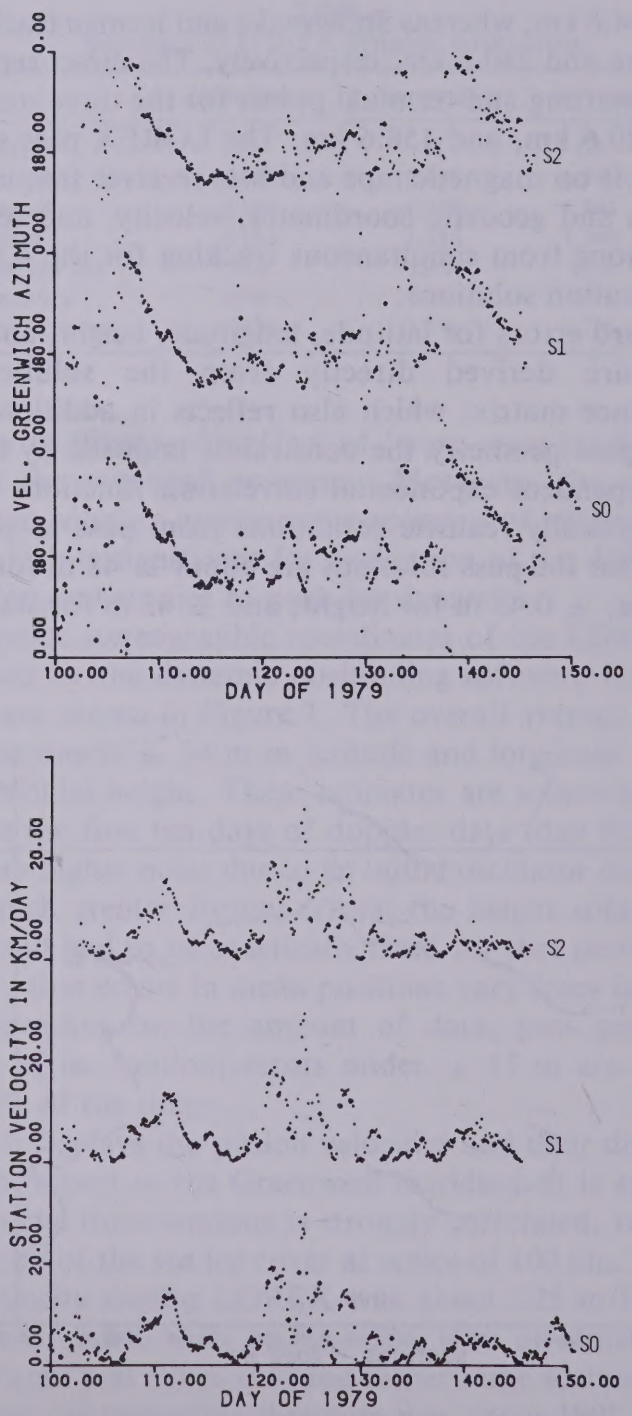

Figure 2. LOREX station velocity plots.

aration. These figures are again somewhat conservative due to the inclusion of the noisy data from the first ten days of the expedition, but they agree well with the errors given above for the three-hour mean positions. The slightly smaller error for station separation provides an independent check, as the accuracy of the relative station positions is free of orbit-related biases. The station velocities and the Greenwich azimuths of the motion have been evaluated as a three-pass running average based on consecutive station pass solutions. They show a higher mean value of about 270 m/h compared to 225 m/h derived from the station mean positions. This very likely reflects the short-period variation in ice motion, which is probably a major factor limiting the achievable accuracy of the results.

Ellipsoidal Heights

The simultaneous three-dimensional solution provides geometrical heights of the electrical centers of receiving antennae above the reference ellipsoid. The height time series (Figure 3) show a remarkable correlation of station height variations from day 109 on. These have amplitudes from 0.2 to about 4 m and range from one-day events to systematic trends clearly dominating any changes in height differences between the stations. Figure 3 does not contain any correction for antenna height, and it seems to reflect clearly the fact that the antenna at the Main Camp (S0) was located on the roof of the navigation hut about 2.30 m above the ice surface, whereas the Iceman antenna (S2) was placed on a small transport box only about 0.45 m high. Since it had not been anticipated that station ellipsoidal heights could be evaluated from satellite data, the antenna heights above water were not measured in the field. Approximate heights above ice have been determined from photographs of the antennae taken in the field, and it is estimated that the uncertainty of the height above water is less than 0.3 m.

The maximum sea surface slope and its Greenwich azimuth have been evaluated from the corrected mean three-hour ellipsoidal heights of the LOREX stations (Figure 4). This regional sea-surface slope with respect to the reference ellipsoid shows rather small variations between 5″ and 15″, with the mean Greenwich azi-

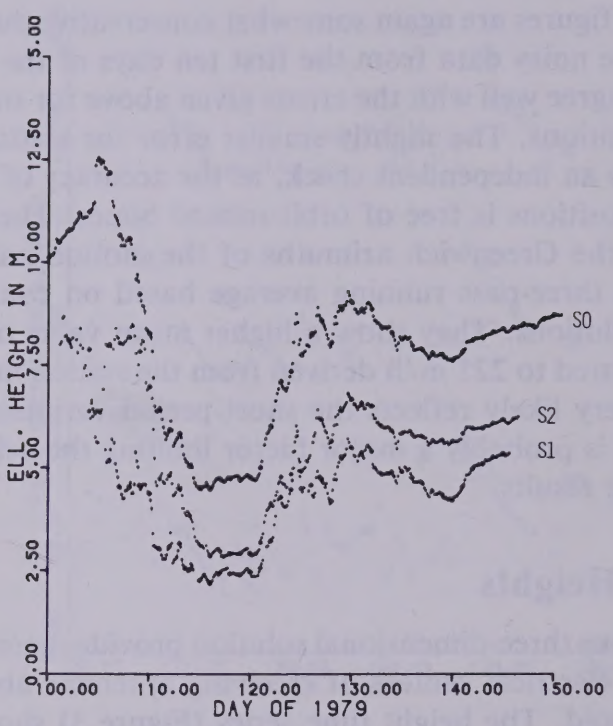

Figure 3. Mean three-hour ellipsoidal heights of LOREX ice camps.

muth of about 37°. However, such a slope would produce a general reduction of ellipsoidal heights for the LOREX stations along their paths, which is inconsistent with the results showing significant increase after day 121 (Figure 3). The discrepancy indicates the presence of a large time-varying component of the computed ellipsoidal heights common to the three stations. There are two possible sources of such variations: (1) the first relates to variations of the instantaneous sea ice surface resulting from dynamics of the ocean, atmosphere, and pack ice; and (2) the second would reflect systematic effects due to satellite orbital biases and data-reduction model deficiencies. While the former group would be of considerable interest to oceanographic studies, the latter represents disturbances that cannot be eliminated easily in the present data set. However, satellite-related effects are considered small, since precise orbits have been used for three of the five satellites,

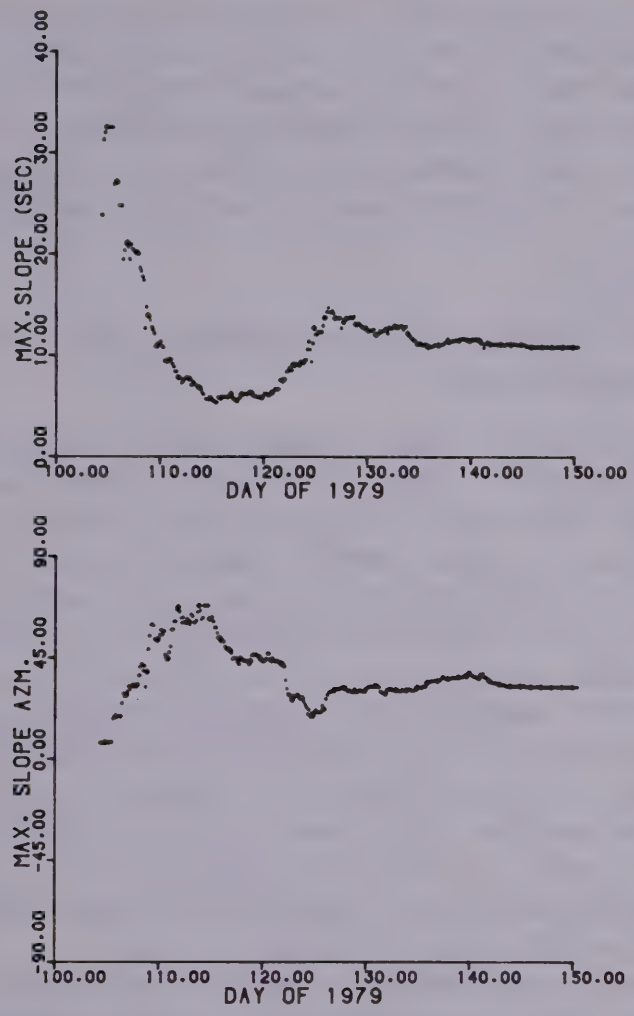

Figure 4. Regional sea-surface slope with respect to the reference ellipsoid.

and the error-modeling procedures have produced consistently high precision results for routine geodetic satellite surveys in similar circumstances. Only the possibility of highly anomalous ionospheric conditions in the polar region may be of some concern; it would be therefore highly desirable to include one or two land stations in future adjustments of sea ice stations and properly constrain the height solution.

Many short-term variations in ellipsoidal height can be correlated with changes in horizontal station velocities (Figure 2) and the horizontal pack ice strain discussed below. The sudden increase of the station ellipsoidal heights starting on day 121 correlates with a sharp decrease of the surface water salinity and a small increase in water temperature reported at Iceman by Pounder (1980).

Differential Station Motion and Sea Ice Deformation Model

It is apparent from the shapes of the LOREX triangle as shown for day 109 and 145 in Figure 5 that considerable deformation and rotation have taken place. The nature of the deformation is revealed by changes in relative station positions as given by lengths and orientation of the sides of the triangle (Figure 6). The side connecting the Main Camp and Snowsnake (S0–S1) shows little change in station separation before day 118 and after day 127, while nearly 2-km extension followed by about 4-km contraction took place in between; it is of interest that the side was approximately parallel with and crossing the Lomonosov Ridge at the time. The side also shows rather steady clockwise rotation of more than 15°. The other two sides clearly indicate episodic extension taking place in the direction roughly perpendicular to the Lomonosov Ridge with a generally smaller rotation.

Sea ice deformation includes opening of leads, formation of pressure ridges, and shear displacement along cracks and leads. These approximately linear features display locally large velocity variations and discontinuities. However, on a sufficiently large scale the pack ice sheet can be treated as a continuum, assuming large numbers of floe-to-floe discontinuities with no single one excessively long (Maykut et al., 1972; Coon et al., 1974; Thorndike and Cheung, 1977). The pack ice sheet deformations are evaluated in two-dimensions due to the great difference between horizontal scales ($\sim$1,000 km) and vertical scales ($\sim$10 m), and because horizontal velocities are basically constant throughout the thickness of any particular ice floe. The polar stereographic co-

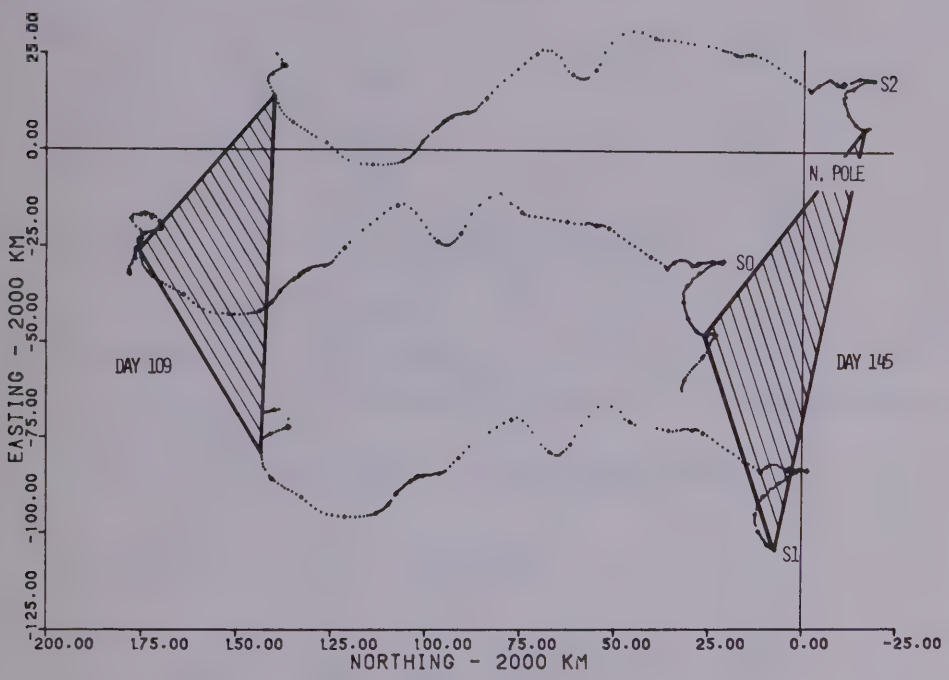

Figure 5. LOREX triangle deformation due to differential sea ice drift between days 109 and 145 of 1979.

ordinates X–northing and Y–easting have been used for the strain analysis.

The following mathematical model has been adopted to express displacements v_{xj} and v_{yj} of station j in the X and Y coordinates:

$$v_{xj} = \frac{\partial v_x}{\partial x} {}_j x_i + \frac{\partial v_x}{\partial y} {}_j y_i + X_{oj}$$

$$v_{yj} = \frac{\partial v_y}{\partial x} {}_j x_i + \frac{\partial v_y}{\partial y} {}_j y_i + Y_{oj} \qquad (1)$$

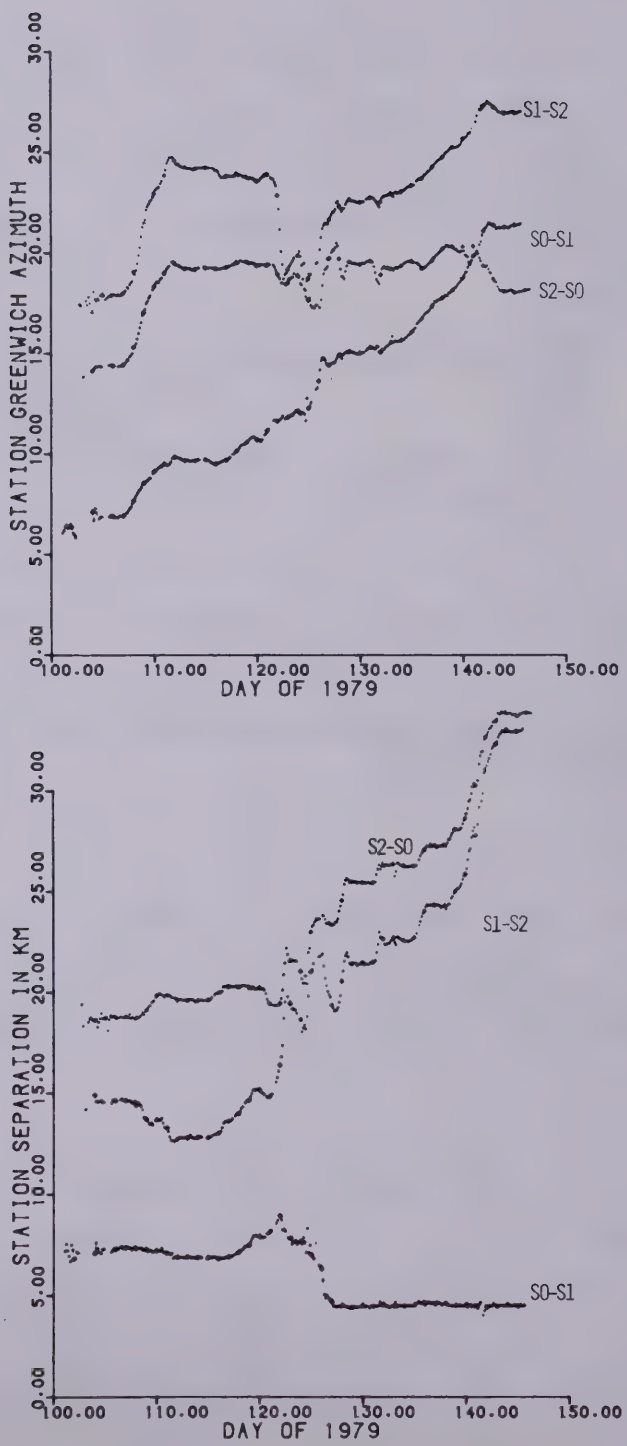

Figure 6. Relative changes of the LOREX triangle side lengths and orientation.

where

$v_{xj} = X_j(t) - X_j(0)$
$v_{yj} = Y_j(t) - Y_j(0)$
$x_i = X_i(0) - X_j(0)$
$y_i = Y_i(0) - Y_j(0)$
i, j = 1, 2, . . ., n number of stations

$[(X_j(t), Y_j(t)]$ and $[X_j(0), Y_j(0)]$ represent the current and initial positions of station j

$\partial v_x/\partial x$, $\partial v_y/\partial x$, $\partial v_x/\partial y$, $\partial v_y/\partial y$ are corresponding displacement gradients

X_{oj}, Y_{oj} are constants representing the translation

Equation (1) can be expressed as

$$v_j = e r_i + c_j \qquad (2)$$

where

v_j is the displacement vector, r_i is the position vector, c_j is the translation component of the displacement vector and e represents the deformation tensor matrix. Thus, according to Equation (2), e serves as a transformation matrix from the position vector to the displacement vector and represents a distortion and/or rotation of a body. Elements of the deformation tensor and the translation components are obtained from the two sets of linear Equations (1), providing coordinates and displacements of at least three suitably distributed stations are known. If more than three stations are involved, a least-squares solution can be obtained assuming homogeneous strain in the region under consideration.

The nontranslational deformation tensor e defined by the displacement gradients can be expressed as the sum of a symmetrical and an asymmetrical tensor

$$e = \epsilon + \omega$$

with elements

$$\epsilon_{k1} = \tfrac{1}{2}(e_{1k} + e_{k1}) = \epsilon_{1k}$$

$$\omega_{k1} = \tfrac{1}{2}(e_{1k} - e_{k1}) = -\omega_{1k}$$

The first part defines the symmetric strain tensor

$$\underline{\varepsilon} = \begin{bmatrix} \varepsilon_{xx} & \varepsilon_{xy} \\ \varepsilon_{xy} & \varepsilon_{yy} \end{bmatrix} = \begin{bmatrix} \frac{\partial v_x}{\partial x} & \frac{1}{2}\left(\frac{\partial v_x}{\partial y} + \frac{\partial v_y}{\partial x}\right) \\ \frac{1}{2}\left(\frac{\partial v_x}{\partial y} + \frac{\partial v_y}{\partial x}\right) & \frac{\partial v_y}{\partial y} \end{bmatrix} \tag{3}$$

and the second part is the pure rotation

$$\underline{\omega} = \begin{bmatrix} 0 & \omega \\ -\omega & 0 \end{bmatrix} = \begin{bmatrix} 0 & \frac{1}{2}\left(\frac{\partial v_x}{\partial y} - \frac{\partial v_y}{\partial x}\right) \\ -\frac{1}{2}\left(\frac{\partial v_x}{\partial y} - \frac{\partial v_y}{\partial x}\right) & 0 \end{bmatrix} \tag{4}$$

The ϵ_{xx} and ϵ_{yy} strain components represent extension along the X and Y axes, whereas $2\epsilon_{xy}$ gives the simple shear. Characteristics values (the eigen values) of the strain tensor ϵ define the maximum and minimum strain, also called principal strains and their directions. These coincide with axes of the strain ellipse representing the irrotational part of the nontranslational two-dimensional deformation. Strain invariants are given by

$$\epsilon_I = \epsilon_{xx} + \epsilon_{yy} \tag{5}$$

called dilatation (or divergence) and

$$\epsilon_{II} = [(\epsilon_{xx} - \epsilon_{yy})^2 + 4\epsilon_{xy}^2]^{1/2} \tag{6}$$

representing maximum shear.

The above theory holds for infinitesimal strain characterized by small displacement gradients for which the squares and products are negligible. However, progressive pack ice deformation shows

considerable displacement gradients even for incremental strain over time intervals of a few hours. Therefore, the general linear transformation

$$\begin{bmatrix} x' \\ y' \end{bmatrix} = \begin{bmatrix} a & b \\ c & d \end{bmatrix} \begin{bmatrix} x \\ y \end{bmatrix} \tag{7}$$

is used to relate the final position (x', y') of a particle after deformation to its initial position (x, y). It is easy to show that the strain components can be expressed in terms of the transformation matrix elements as follows:

$$\begin{aligned} \epsilon_{xx} &= a - 1 \\ \epsilon_{xy} &= \tfrac{1}{2}(b + c) \\ \epsilon_{yy} &= d - 1 \\ \omega &= \tfrac{1}{2}(b - c) \end{aligned} \tag{8}$$

The finite homogeneous strain components are then evaluated from the following expressions:

$$\begin{aligned} \text{dilatation:}\quad & \epsilon_{I} = ad - bc - 1 \\ \text{max. shear:}\quad & \epsilon_{II} = \left[(a-d)^2 + (b+c)^2\right]^{\frac{1}{2}} \\ \text{max. strain:}\quad & \epsilon_{MX} = \tfrac{1}{2}\left[a+d + \left[(a-d)^2 + (b+c)^2\right]^{\frac{1}{2}}\right] - 1 \\ \text{min. strain:}\quad & \epsilon_{MN} = \tfrac{1}{2}\left[a+d - \left[(a-d)^2 + (b+c)^2\right]^{\frac{1}{2}}\right] - 1 \\ \text{MX direction:}\quad & \Phi = \tan^{-1}\left[\frac{b+c}{a-d + \left[(a-d)^2 + (b+c)^2\right]^{\frac{1}{2}}}\right] \end{aligned} \tag{9}$$

The mean three-hour station positions have been used for evaluating strain components. The polar stereographic station coor-

dinates for day 105 at 15/ UT define the initial "undeformed" triangle configuration. At that moment reliable continuous satellite doppler data became available from all three LOREX stations. The strain monitoring continued until day 145 at 15/ UT when the Snowsnake station satellite tracking terminated.

Progressive Sea Ice Deformation—Total Strain

The total strain components for the LOREX triangle have been obtained by comparing station configurations with the initial "undeformed" state, using the expressions (7) to (9) for finite homogeneous strain. Figure 7 shows the nonrotational strain components with respect to the polar stereographic axes. Direction of the maximum strain and the principal strains are shown in Figure 8, whereas the pure rotation, maximum shear, and dilatation are plotted in Figure 9. The progressive pack ice and deformation is well defined from the LOREX triangle, and two distinct deformation patterns can be identified. The first between day 110 and 120 is characterized by relatively small deformations with direction of the maximum strain nearly parallel with the Greenwich meridian. The second pattern from day 127 on displays progressive steplike extension in the direction approximately perpendicular to the Lomonosov Ridge with increasing dilatation. The two transition periods (before day 110 and between day 120 and 127) show rapidly changing direction of the axis of the maximum strain, and while the first transition indicates significant dilatation the second displays just the opposite, i.e., divergence of about the same magnitude. Systematic rotation by several degrees in opposite directions is also observed during the two transitions. Day 121 marks the most dramatic changes, and interestingly enough it coincides with the breakup of the Main Camp that was crossing the crest of the Lomonosov Ridge at the time. Moreover, as mentioned above, a significant drop in surface water salinity was recorded at Iceman, and a major increase of sea surface heights occurred at all three stations (Figure 3). These facts can be interpreted in terms of distinctly different hydrographic regimes in the Canadian and Eurasian basins adjacent to the Lomonosov Ridge (Aagaard, 1981). However, one cannot rule out a transient event

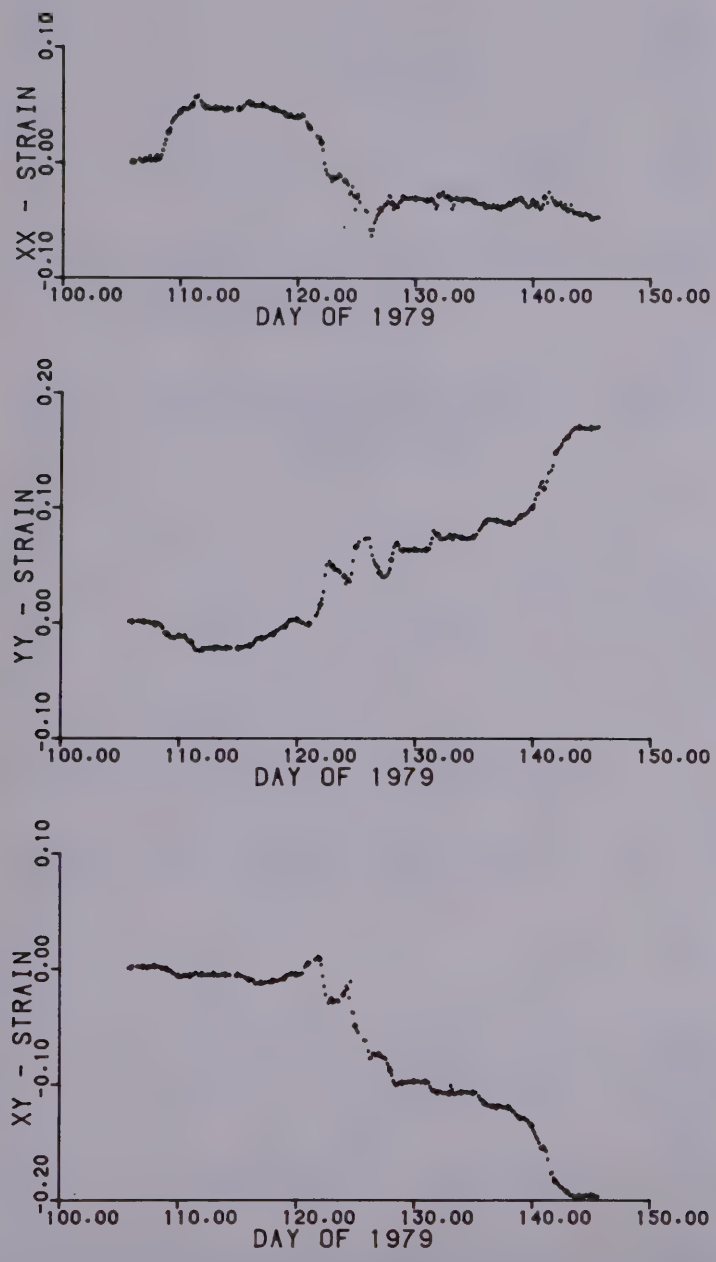

Figure 7. Nonrotational total strain components.

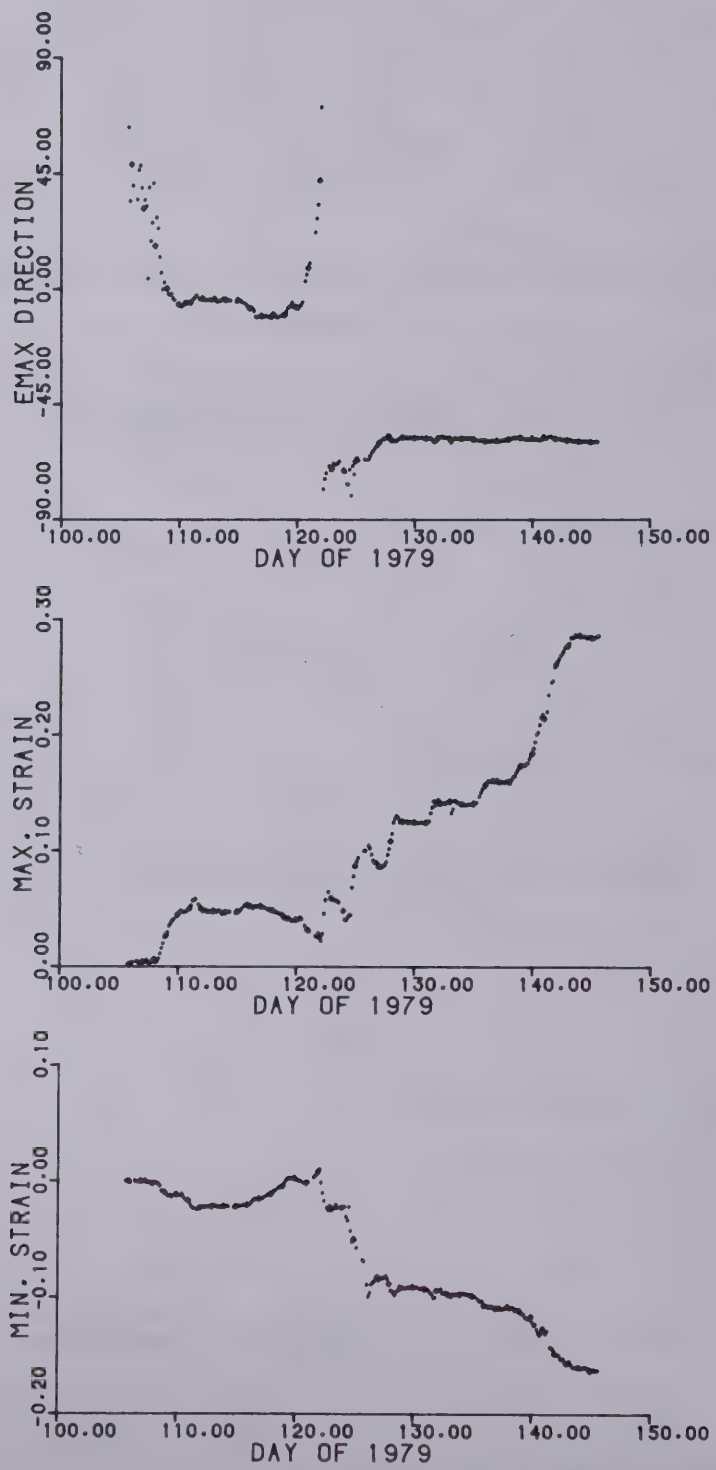

Figure 8. Principal total strain components and their orientation.

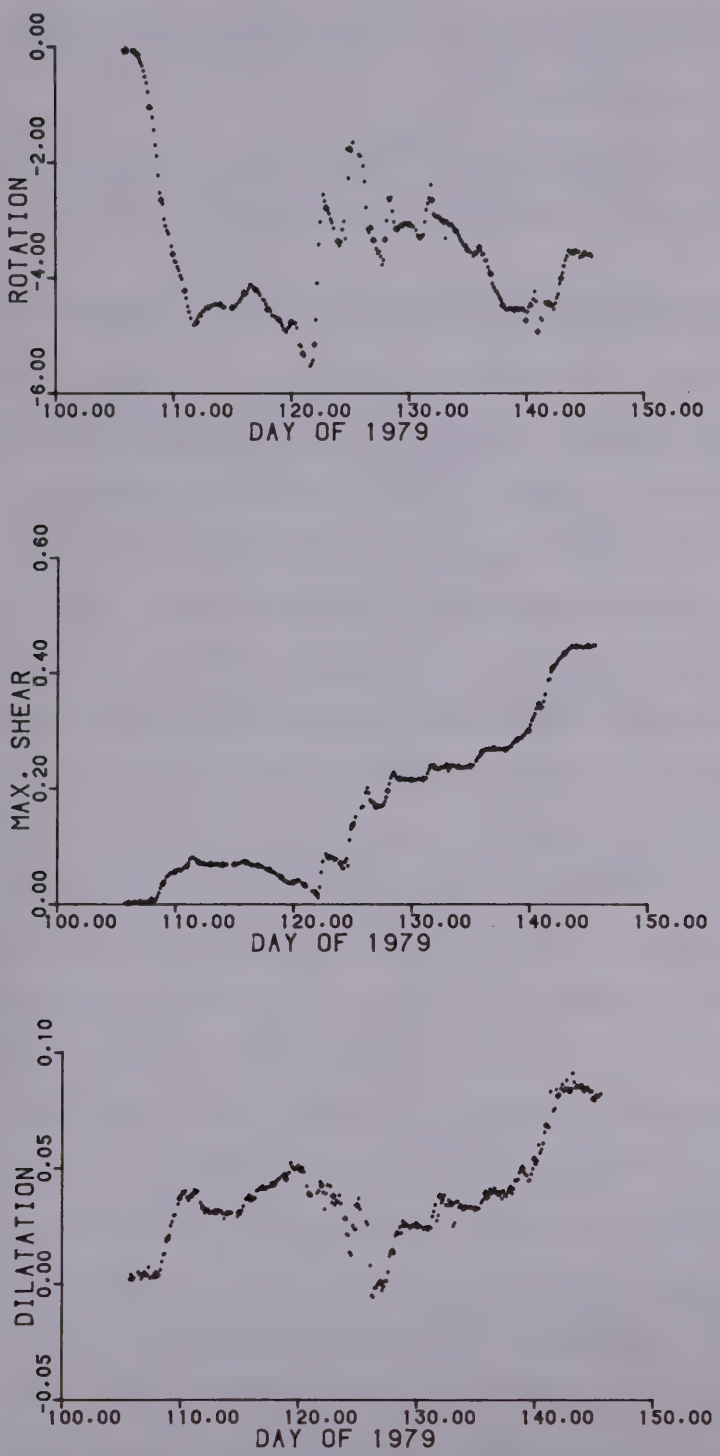

Figure 9. Pure rotation, maximum shear, and dilatation for total deformation.

as a possible source no matter how unlikely the coincidence with crossing of the ridge might be. Only additional new data could resolve the ambiguity.

In general, the total deformation during the 40-day period is considerable and reaches nearly 30% for maximum strain, exceeds 8% for dilatation, and shows pure rotation up to 5.5°.

Incremental Sea Ice Deformation — Strain Rate

The strain rate calculations are based on differences of consecutive mean three-hour station positions. Since the magnitude of differential strain effects for three-hour intervals is only marginally larger than the uncertainty in the mean station positions and both can vary a great deal, it is important to consider the known formal position errors when evaluating the strain rate components. This has been done by independent least-squares cubic spline smoothing of the elements of the transformation matrix in Equation (7), with weights reflecting the formal errors of station positions. The incremental strain components computed from the expressions (8) and (9) have been scaled to represent strain rates per hour, and these are shown in Figure 10 for the nonrotational components, whereas Figures 11 and 12 show the principal strain rates, hourly changes in dilatation, maximum shear, and pure rotation.

The major events reflecting large-scale permanent deformations clearly defined by the total strain (Figures 8 and 9) are expressed by conspicuous narrow anomalies of the strain-rate components, which permit more accurate determination of their timing and character. Often rapid, large changes in one direction are followed by somewhat lesser change in the opposite direction. Under close examination regular, nearly diurnal variations of the strain rate components can be observed between the major events. Most noticeable are these variations in the dilatation rate between day 112 and 120. Some correlation between strain rate components and the fine submeter ellipsoidal height variations (Figure 3) also can be observed. Detailed strain and tilt observations on a single large ice floe should be considered in the future to determine if this oscillation is related to elastic ice deformation due to tidal forces. In any case, additional observations are necessary to establish the

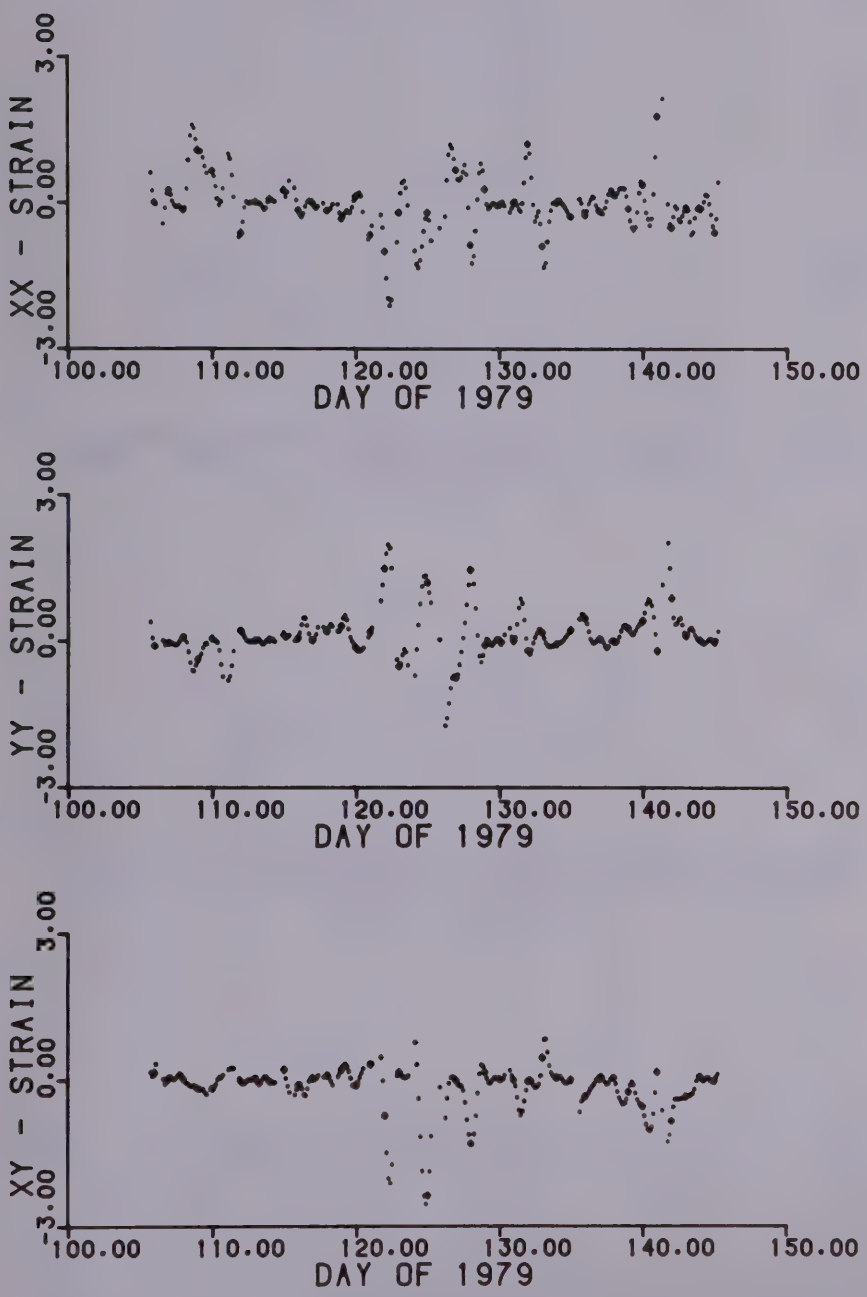

Figure 10. Nonrotational strain rate per hour (units of 10^{-3}).

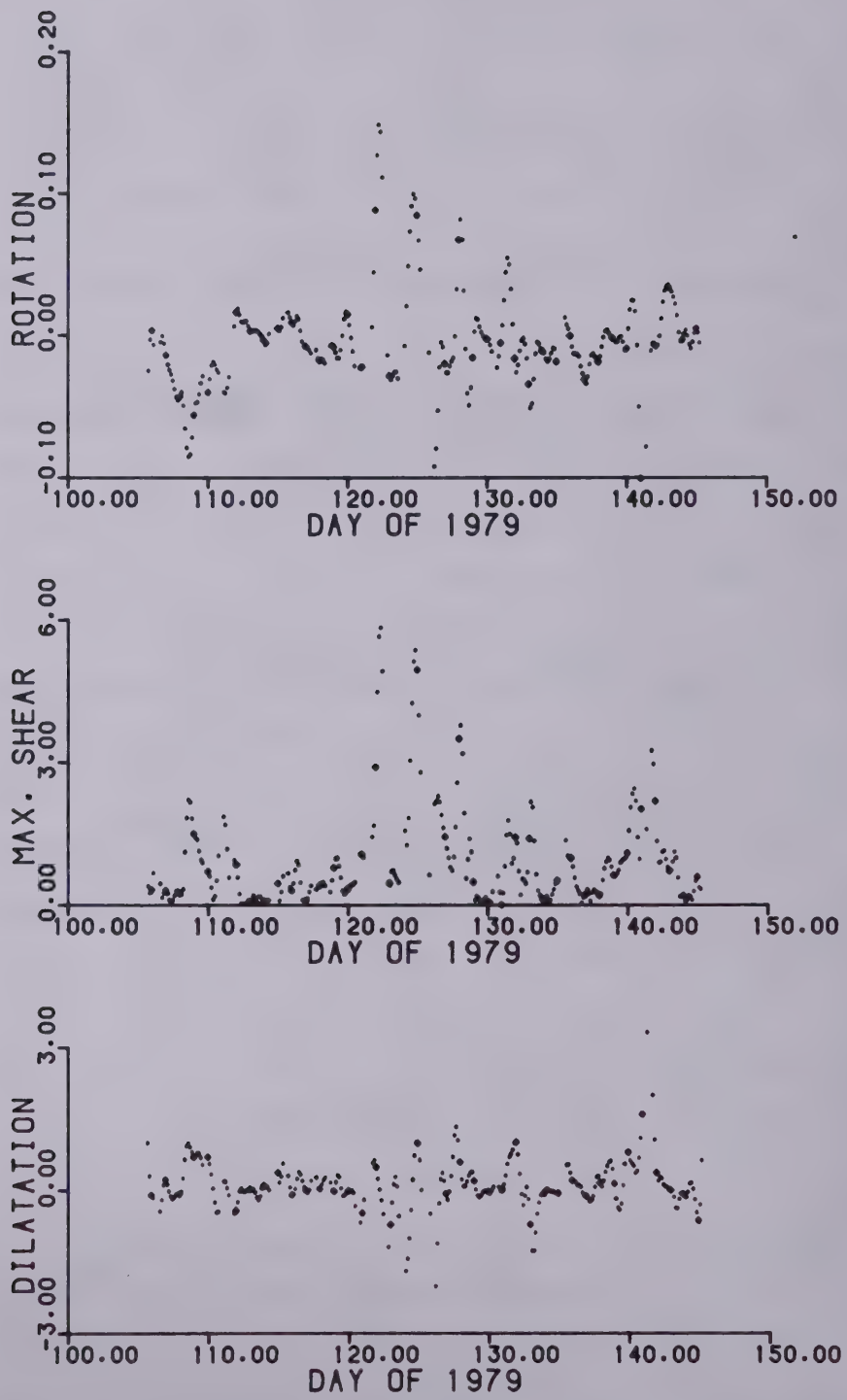

Figure 11. Hourly rates of pure rotation (in degrees), maximum shear, and dilatation (units of 10^{-3}).

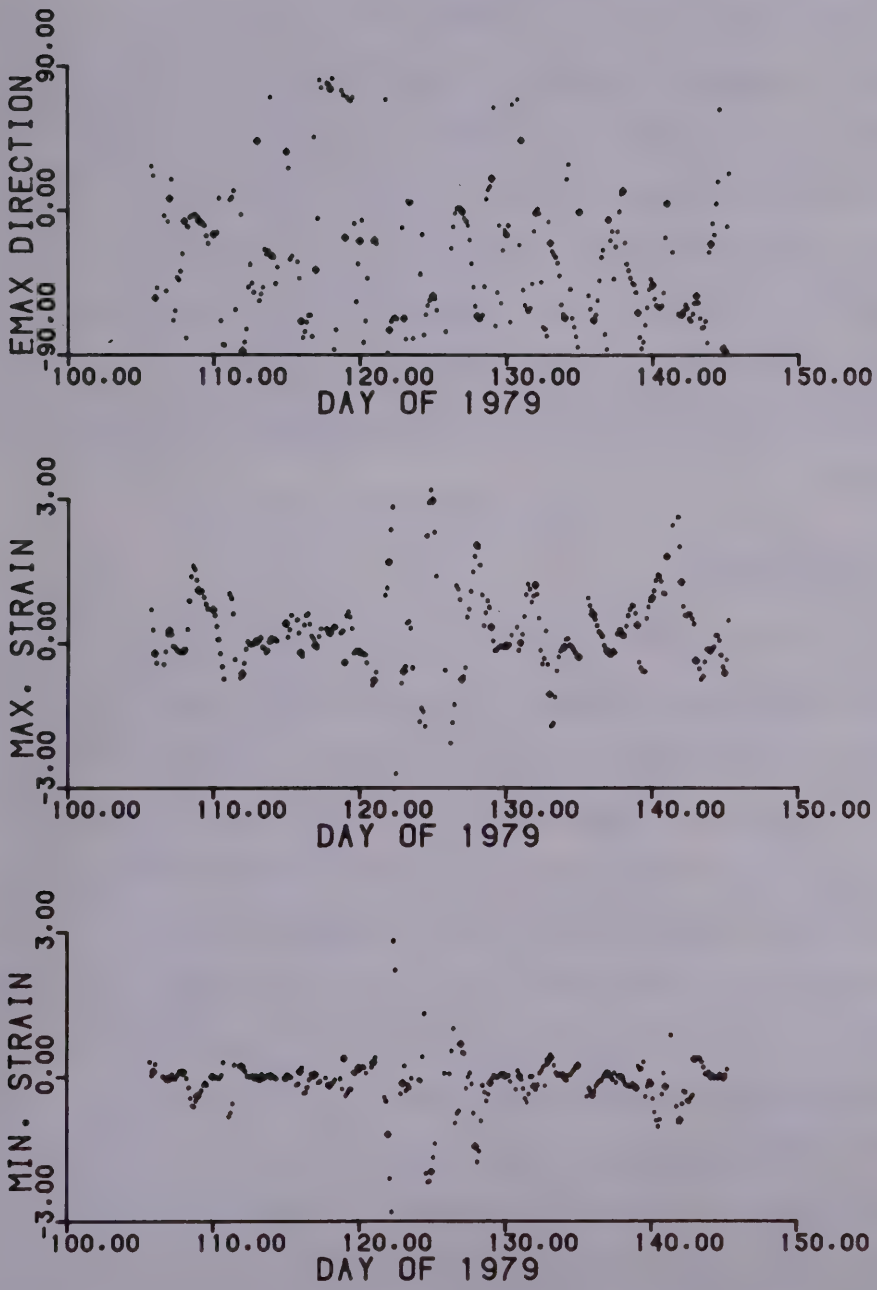

Figure 12. Principal strain rates per hour (units of 10^{-3}) and their orientation.

suitability of the two-dimensional homogeneous strain model and evaluate the effect of large discontinuities between the floes on the computed strain components.

The anomalous hourly changes have reached about 0.3% for maximum strain and dilatation, whereas maximum hourly change in pure rotation has been 0.15°. The above-mentioned nearly diurnal variations of the same components show amplitudes about an order of magnitude smaller. The greatest variance is displayed by the direction of maximum strain, which shows signs of discontinuous systematic trends, particularly in the second half of the experiment. An analysis of statistical frequency produces two peaks: one around $-65°$ and one somewhat broader and smaller around $-10°$. The average hourly changes over the duration of the experiment amount to 0.024% extension for maximum strain and 0.011% dilatation, which is consistent with the total deformation results.

Conclusions

The Navy Navigation Satellite System facilitates reliable real-time navigation for drifting ice stations in the vicinity of the geographic North Pole. The positional accuracy can be improved significantly using postfitted precise satellite ephemeris and the newly developed dynamic doppler data reduction software. The new software accommodates multistation three-dimensional sequential positioning of slowly moving platforms under the assumption of linear motion over specified equal-length time intervals. It reflects time and space correlation of model parameters, including environmental and instrumental effects, station coordinates, and mean interval velocities. The sequential adjustment scheme updates all model parameters and corresponding variance–covariance matrices after each satellite pass, assuring data manageability and exceptional economy of computations. In this way all 2,700 satellite passes have been reduced in one computer run, using three-hour intervals to approximate station drift by linear motion. The overall average error of the mean three-hour station positions is less than $\pm$ 25 m in horizontal coordinates and about $\pm$ .4 m in ellipsoidal height, while the average station velocity was about 225

m/h with the maximum of 1,240 m/h. The average error of the 4,836 individual pass-station solutions derived directly from the variance–covariance matrices is less than ± 50 m in horizontal coordinates and ± .45 m in height, probably reflecting the high frequency ice jerk.

The positional accuracy is sufficient to monitor progressive pack ice deformation using a two-dimensional homogeneous strain model. The configuration of the three LOREX ice camps provides a unique solution for total mesoscale strain, indicating that a major change in the ice deformation pattern takes place above the Lomonosov Ridge in the vicinity of the North Pole. It is characterized by a change in the direction of maximum strain of more than 50° and clear divergence when crossing the ridge. The total strain reflects mostly plastic deformation, which takes place mainly in episodic events when the ice yields under the effects of shear and vertical stress.

Analysis of strain rate can be enhanced by smoothing of observations, which takes into account formal errors of individual mean station positions. The strain rate components produce conspicuous anomalies corresponding to the major deformation events. Moreover, nearly diurnal oscillations with an order of magnitude smaller amplitude are quite apparent. However, their interpretation would have to include detailed analysis of the suitability of a two-dimensional homogeneous strain model for pack ice deformation studies, which can only be based on presently unavailable redundant observations.

Similarly, the interpretation of ellipsoidal heights would require at least one land-based station to be included with the ice stations in the simultaneous adjustment to constrain the height solution. Additional monitoring of oceanographic and meteorological parameters is necessary to identify sources of pack ice motion and deformation. Future expeditions could provide more information by optimizing satellite-observing strategy to assure sufficient redundancy of measurements and by obtaining complementary geodetic, oceanographic, and meteorological data to study the interactions between the ocean and atmosphere, which determine ice conditions. This would also be beneficial to other scientific projects and contribute greatly to the safety of operations.

Acknowledgments

The authors are deeply obliged to Dr. D. Wells who conceived and set up the satellite navigation and the near real-time fix evaluation on the ice with support from F. Muise and S. Spencer of the Bedford Institute of Oceanography. Many thanks go to the LOREX Chief Scientist, Dr. J. R. Weber, and to the management of the Earth Physics Branch for advice, support, and encouragement, which have made the work possible. The cooperation of the U.S. Defense Mapping Agency Topographic and Hydrographic Center in providing the precise postfitted satellite ephemeris is gratefully acknowledged.

References

Aagaard, K. 1981. On the Deep Circulation in the Arctic Ocean. *Deep-Sea Research*, 28A (3).

Coon, M. D., Maykut, G. A., Pritchard, R. S., Rothrock, D. A., and Thorndike, A. S. 1974. Modelling the Ice Pack as an Elastic-Plastic Material. *AIDJEX Bull.* No. 24.

Johnson, G. W. 1982. Astronavigation for the Lomonosov Ridge Experiment. Manuscript.

Kouba, J. 1979. Improvements in Canadian Geodetic Doppler Programs. *Proc. 2nd Symp. on Satellite Doppler Positioning*, Las Cruces.

Kouba, J. 1981. Satellite Doppler Positioning for Geodynamics. *Proc. Symp. on Space Geodesy, Annales de Geophysique*, 37, (1).

Kouba, J., and Boal, J. D. 1976. Program GEODOP. Publ. Surveys and Mapping Branch, Ottawa.

Maykut, G. A., Thorndike, A. S., and Untersteiner, W. 1972. Aidjex Scientific Plan. *AIDJEX Bull.* No. 15.

Popelar, J., Kouba, J., and Wells, D. E. 1981. LOREX 79 Satellite Positioning. Internal Report 81-2, Gravity & Geodynamics Division, Earth Physics Branch, E.M.R.

Pounder, E. R. 1980. Physical Oceanography in the Central Arctic. Manuscript.

Thorndike, A. S., and Cheung, J. Y. 1977. AIDJEX Measurement of Sea Ice Motion 11 April 1975 to 14 May 1976. *AIDJEX Bull.* No. 35.

Weber, J. R. 1979. The Lomonosov Ridge Experiment: LOREX 79. *Trans. AGU*, No. 42.

Wells, D. E. 1976. Improved Marine Navigation Error Modelling Through System Integration. *CGU Symposium on Modern Trends in Geodesy*, Quebec.

Wells, D. E., and Grant, S. T. 1977. Reliable Navigation Through System Integration. *Proc. 16th Can. Hydrographic Conference*, Burlington.

Date Due

54670

Pam:551.326.14:
(*301)
POP

POPELAR, J. and KOUBA, J.

AUTHOR

Satellite doppler determination

TITLE of differential sea ice
motion in the ...

DATE LOANED	BORROWER'S NAME	DATE DUE

54670

BOREAL INSTITUTE FOR NORTHERN STUDIES, LIBRARY
THE UNIVERSITY OF ALBERTA
EDMONTON, ALBERTA T6G 2E9
CANADA

University of Alberta Library
0 1620 0332 6244